

Mallard Blue binding to heparin, its SDS micelle-driven de-complexation, and interaction with human serum albumin: A combined experimental/modeling investigation

Domenico Marson ^a, Erik Laurini ^{a, *}, Maurizio Fermeglia ^a, David K. Smith ^b, Sabrina Pricl ^a

^a Molecular Simulation Engineering (MOSE) Laboratory, Department of Engineering and Architecture (DEA), University of Trieste, Piazzale Europa 1, 34127 Trieste, Italy

^b Department of Chemistry, University of York, Heslington, York, YO10 5DD, United Kingdom

ARTICLE INFO

Keywords:

Mallard Blue
Heparin sensor
SDS micelles
Molecular simulations
Experimental validation

ABSTRACT

Heparin is a sulfated glycan widely used as anticoagulant in medicine. Mallard Blue (MalB), a small cationic dye developed in our laboratories, is able to detect heparin in serum and plasma in a dose-response manner, with performance superior to its direct competitors. However, many aspects of MalB/heparin binding still remain to be explored which, once solved, may foster the clinical use of MalB. Among these, the characterization of the energetics that drives the MalB/heparin binding process, the competition for MalB binding by other polyanions (e.g., negatively-charged surfactant micelles), and the interaction of MalB with serum proteins are of particular interest. This work fills this gap by means of a combination of experimental investigations (UV-visible spectroscopy and isothermal titration calorimetry), and computational approaches based on molecular dynamics (MD) simulation techniques. In combination, the results obtained show that MalB efficiently binds to both heparin and SDS, with the binding being enthalpic in nature; yet, SDS is able to extract MalB from its complex with heparin when the surfactant is in its self-assembled form, the driving force underlying SDS-induced MalB/heparin de-complexation being entropic in nature as the two enthalpies of binding effectively cancel each other out. Once bound to SDS, the dye remains electrostatically bound to the micellar surface and does not penetrate the micelle palisade layer, as verified by steered molecular dynamics/umbrella sampling simulations. Finally, the affinity of MalB for human serum albumin (HSA), the most abundant plasma protein, is found to be lower than that for heparin, confirming the ability of the dye to work in complex physiological environments.

1. Introduction

Heparin, a linear polysaccharide consisting of repeating units of 2-O-sulfated iduronic acid and 6-O-sulfated, N-sulfated glucosamine (IdoA(2S)-GlcNS(6S), Fig. 1 left) – is one of the most charge-dense naturally occurring polyanion in biological systems [1]. Heparin has been used as an anticoagulant since 1935 to both treat and prevent the deep vein thrombosis that can result from large surgery, blood transfusions, or dialysis. As a result of its clinical importance, there has been a surge of interest in developing

heparin sensors which can directly detect heparin chains within a complex biological sample (that is, measure a true concentration) rather than rely on an activity measurement within plasma or serum (units of anticoagulant activity). Perhaps the leading strategy has been the development of cationic indicator dyes which can quickly report on heparin spectroscopically. In this respect, several molecules such as Azure A [2,3], Alcian Blue [4], Methylene Blue [5], Heparin Blue and Heparin Orange [6] – which all exhibit UV response to heparin – have historically been employed. Yet, while these cationic dyes work well in noncompetitive environments, many of them lose efficiency a) in the presence of other agents (e.g., plasma proteins) that directly interfere with their heparin non-covalent binding and b) as electrolytic competition increases.

In the quest for alternative heparin sensors that can quantitatively and reliably perform under physiological conditions, in 2013

* Corresponding author.

E-mail addresses: domenico.marson@dia.units.it (D. Marson), erik.laurini@dia.units.it (E. Laurini), maurizio.fermeglia@dia.units.it (M. Fermeglia), david.smith@york.ac.uk (D.K. Smith), sabrina.pricl@dia.units.it (S. Pricl).

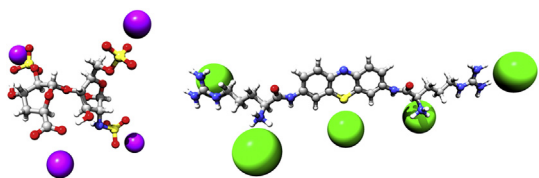


Fig. 1. Molecular model of the predominant average repeat unit of heparin (left) and of Mallard Blue (MalB, right). In each structure, the molecules are shown as atom-colored sticks-and balls (C, gray; O, red; N, blue; S, yellow; H, white). Na⁺ and Cl⁻ counterions are portrayed as purple and green spheres, respectively. (For interpretation of the references to colour in this figure legend, the reader is referred to the web version of this article.)

our group synthesized Mallard Blue (MalB, Fig. 1 right), a thionine-arginine molecule that can be readily obtained via a coupling reaction between Tri-Boc-protected arginine and thionine acetate followed by Boc deprotection [7].

In the same study [7], we established that MalB is able to detect heparin in serum and plasma in a dose-response manner, its superior performance with respect to the direct competitor Azure A, its heparin specificity and, likely its most interesting and promising property, its resistance to high ionic strength (e.g., 150 mM NaCl), despite the fact that electrostatic forces govern its interaction with the polyanion. Interestingly, the excellent sensing properties of MalB under physiological conditions were the subject of a positive *News and Views* article which appeared in *Nature Chemistry* in the same year [8].

Under this promising scenario, however, many aspects still remain to be explored which, once solved, may foster the clinical use of MalB. Among these, the characterization of the energetics that drive the MalB/heparin binding process, the competition for MalB binding by other polyanions (e.g., negatively-charged surfactant micelles), and the interaction of MalB with serum proteins still remain to be performed. This work aims to fill this gap by means of a combination of experimental investigations, based on UV-visible spectroscopy and isothermal titration calorimetry (ITC), and computational approaches, relying on molecular dynamics (MD) simulation techniques.

Specifically, since the interaction of MalB with heparin has never been fully characterized so far, either from a spectrometric or from a thermodynamic point of view, we first report and discuss the spectroscopic and thermodynamic behavior for MalB binding to heparin and compare them with that obtained for negatively-charged micelles generated by the self-assembly of a conventional anionic surfactant sodium dodecyl sulfate (SDS). The idea underlying these experiments is that, given the predictable electrostatic nature of heparin/MalB interaction, highly oppositely-charged micelles may compete with the polysaccharide and promote MalB dissociation with subsequent sequestration. Indeed, micelle-assisted “extraction” of bound ligands from polyanions is a competitive phenomenon, particularly in the case of DNA (e.g., drugs/mutagens DNA de-intercalation). However, the energy cost for such processes is still not properly understood. Therefore, we deemed it very interesting to investigate this particular aspect in case of MalB. These experiments are paralleled by computational investigations based on steered molecular dynamics [8–12], which allow us to mimic MalB unbinding from heparin and subsequent association with SDS micelles at a molecular level.

Next, we present the results of binding thermodynamics of MalB to the most representative plasma protein, human serum albumin (HSA), and resort again to atomistic MD simulations in the Molecular Mechanics/Poisson-Boltzmann framework of theory [see 13–16 and references therein] to identify the molecular determinants underlying its interaction with the heparin sensor.

2. Materials and methods

All chemicals were purchased from Sigma Aldrich, and used without further purification. Mallard Blue, heparin and human serum albumin were available from our previous work [7,17–22].

2.1. UV-visible spectroscopy

UV-visible absorbance was measured on a DeNovix DS11-FX spectrophotometer (DeNovix Inc., Wilmington, DE, USA). All MalB solutions were incubated at 50 °C for 24 h prior to use and stored in the dark. For the MalB/heparin binding, solutions of MalB (125 μM) in 150 mM NaCl and 10 mM Tris HCl were incubated with solutions of heparin at progressively increasing concentrations in the same buffer (9, 17, 34, 67.5, 125, 250, 500, and 1000 μM). For MalB/SDS binding, a series of SDS solutions (0.25, 0.5, 1, 1.5, 2, 3, and 5 mM) were added to the MalB solutions (125 μM, 150 mM NaCl/10 mM Tris HCl). The range of SDS concentrations was selected in order to consider surfactant systems below and above their CMC (1.2 mM, see below). For SDS/MalB binding in the presence of heparin, a presoaked MalB/heparin solution was prepared (125 μM MalB/150 μM heparin, which ensures complete binding [7]) and a series of SDS solutions (0.25, 0.5, 1, 1.5, 2, 3, 5, and 10 mM) were added. All experiments were carried out at 25 °C and performed in triplicate. The absorbance at 615 nm was recorded after each addition.

2.2. Isothermal titration calorimetry (ITC)

2.2.1. Binding of MalB to heparin, SDS micelles, and SDS-driven MalB extraction from heparin

ITC experiments were conducted using MicroCal PEAQ-ITC calorimeter (Malvern, UK) at 25 °C. The cell volume was 280 μL. All experiments were conducted in a backward manner, that is, by step-by-step injections of a constant volume of concentrated heparin or SDS solutions into the calorimetric cell containing buffer (150 mM NaCl/10 mM Tris HCl, pH 7.4), or buffered solutions of MalB, respectively. For SDS-driven MalB extraction from heparin assay, a buffered MalB solution in large excess of heparin (to ensure complete MalB/heparin binding) in the cell was used instead. Specifically, for SDS CMC determination, a constant 1 μL portion of SDS solution (60 mM) was repeatedly injected (37 times) into the reaction cell at 150 s intervals. For MalB binding by heparin, a polyanion solution (2 mM) was injected in 37 portions of 1 μL at 150 s intervals, while the MalB concentration in the calorimeter cell was 125 μM. For MalB/SDS binding, a 1 mM solution of MalB in the cell was titrated with 37 portions of 1 μL of a 300 mM SDS solution at 150 s intervals, such that the concentration of SDS was always above the CMC, and allowing us to make the assumption that the micelles remained intact throughout the experiment. For the MalB/heparin extraction by SDS micelles, the calorimeter cell was filled with a pre complexed MalB/heparin solution (1 mM/5 mM), and titration was performed with a 300 mM solution of SDS (37 portions of 1 μL at intervals of 150 s). All solutions and buffers were degassed for 30 min at room temperature under stirring at 750 rpm prior to each experiment. After careful washing, the cell was pre-rinsed with a portion of the buffer, MalB, or MalB/heparin solutions, respectively. Upon filling the cell and syringe, stirring was turned on and each system was allowed to thermally equilibrate for 30 min. The heat signal resulting from mixing, dilution effects and liquid friction were further confirmed by control experiments (data not shown); accordingly, they were subtracted from the relevant data sets to yield the corrected integrated data. All experiments were run in triplicate.

2.2.2. Binding of MalB to HSA

For this ITC experiment, the instrument cell was filled with a 50 μM buffered (150 mM NaCl/10 mM Tris HCl, pH 7.4) solution of HSA. Titration was performed with a 500 μM buffered solution of MalB, added in 19 portions of 1 μL , with time intervals of 150 s.

2.3. Molecular simulations

2.3.1. Model building, refinement and simulation details

All simulations discussed in this work were carried out using the AMBER16 suite of programs [23], the GAFF force field [24] and performed with the GPU version of *pmemd* (*pmemd.cuda*) in AMBER16 on our MOSE GPU/CPU cluster. AMBER16 is the state of the art simulation platform universally recognized and adopted for simulating biological systems and their interactions with soft matter and small molecules. A SDS micelle (consisting of 60 surfactant monomers) was built using the Micelle Maker server [25], and optimized, following a consolidated procedure for self-assembly nanostructures [17–22,26–30]. The initial, optimized structures of heparin, MalB, heparin/MalB complex and ligand-free human serum albumin (HSA) were taken from our previous work [7,9,14,17–22].

Docking of MalB to HSA was accomplished by adapting a procedure described in details in [[13,15,16,31–34] and references therein]. Briefly, docking experiments were performed with Autodock 4.2/Autodock Tools 1.4.6 [35]. The resulting docked conformations were clustered and visualized; then, only the molecular conformation satisfying the combined criteria of having the lowest (i.e., more favorable) Autodock energy and belonging to a highly populated cluster was selected to carry forward for further modeling. The MalB/HSA complex obtained from the docking procedure was further refined in Amber 16 using the quenched molecular dynamics (QMD) method as previously described [36–38].

The optimized structures of the SDS micelle, heparin/MalB complex, and MalB/HSA complex were immersed in a box of TIP3P water molecules [39]. The choice of the TIP3P model is based on the fact that it is the best compromise between accuracy description of the water behavior and computational time required; moreover, it has been specifically developed and parametrized to simulate hydrated environments of biological macromolecules, surfactants and small organic molecules. The dimensions of each simulation box were chosen in order to ensure a 1 nm solvation shell around each solute structure. Suitable amounts of Na^+ and Cl^- ions required to achieve solution neutrality and realize a physiological ionic strength of 0.15 M were added to each system. The resulting hydrated structures were then subjected to an initial Steepest Descent (SD)/Conjugated Gradient (CG) minimization with 5.0 kcal/(mol \AA^2) restraint on the solute (solvent relaxation), followed by another round of CG minimization without restraints in order to eliminate all bad contacts between water molecules and each solute.

Next, each minimized structure was subjected to molecular dynamics (MD) simulations in the canonical (NVT) ensemble. During these 100 ps of MD, each system was gradually heated and relaxed to 25 $^\circ\text{C}$. The SHAKE algorithm [40] was applied to all covalent bonds involving hydrogen atoms. An integration time step of 2 fs was adopted together with the Langevin thermostat for temperature regulation (collision frequency = 2.0 ps^{-1}) [41]. The final heating step was followed by 50 ns of MD equilibration in the isochoric/isothermal (NPT) ensemble. Pressure control was exerted by coupling the system to a Berendsen barostat (pressure relaxation time 2 ps) [42]. The Particle Mesh Ewald (PME) method [43] was used to treat long-range electrostatic interactions under periodic conditions with a direct space cut-off of 10 \AA . To generate the starting configuration for steered molecular dynamics simulations (Section 2.3.2), a frame of the SDS micelle and of the MalB/heparin

complex was extracted from the corresponding equilibrated MD trajectories. The entire equilibrated MD run of the MalB/HSA complex was used in the determination of dye/protein free energy of binding (section 2.3.3).

2.3.2. Steered molecular dynamics (SMD) and umbrella sampling (US) simulations

The unbinding process of MalB from heparin and the binding event between MalB and the SDS micelle were simulated using a combination of steered molecular dynamics (SMD) [9–12] and umbrella sampling (US) simulations [44]. In the first case, the MalB/heparin complex structure extracted from the corresponding equilibrated MD simulations was solvated with a TIP3P water [39] cubic box, and ions and counter ions were added to neutralize the system and reach the physiological ionic strength (150 mM NaCl). In the second case, the optimized SDS micelle and a molecule of MalB were placed in simulation cell at an initial distance of approximately 5 nm. The resulting system was solvated using the same solvent system adopted for the MalB/heparin complex. After each system equilibration (1 ns of NVT/NPT MD simulation), SMD runs were performed, and were next used to extract the initial coordinates for umbrella sampling simulations along the unbinding/binding pathway, respectively. A pulling force with a virtual spring constant of 50 kcal (mol \AA^2) $^{-1}$ was imposed on the ligand center of mass and the center of mass of the SDS micelle/heparin in the unbinding/binding simulations, and the speed was 5 \AA ns^{-1} based on considerations of sampling accuracy and computational efficiency. The reaction coordinate for the umbrella sampling simulations, ζ , is defined as the distance between the MalB center of mass (COM) and the COM of heparin when pulling MalB out of the heparin complex, and between the COM of MalB and the COM of the SDS micelle when pulling MalB towards the SDS micelle. During both SMD and US simulations, the heparin/SDS micelle initial structures were retained in their initial configurations applying a small constraint force of 5 kcal (mol \AA^2) $^{-1}$ on the coordinates of the heavy atoms of heparin for the unbinding simulations, and on the two terminal carbons of each SDS chain in the binding simulations.

To perform US simulations, MalB position probability distributions along the reaction coordinate were extracted from the corresponding SMD simulations. US method adopts a biased potential function imposed on the structure generated by the SMD along ζ , according to the following equation:

$$U'(\zeta) = U(\zeta) + W(\zeta) \quad (1)$$

Where $U(\zeta)$ is the potential function and $W(\zeta)$ is a quadratic-form weighting function:

$$W(\zeta) = K (\zeta - \zeta_0)^2/2 \quad (2)$$

In which K is the harmonic force constant and ζ_0 is the harmonic potential center.

In this work, each path was subdivided in 80 windows (spacing 0.8 \AA), enough to push the MalB inside the SDS micelle in the binding simulation, and to bring the MalB fairly far away from heparin in the unbinding one. An equilibration time of 1 ns was adopted for each window, and data collection lasted 4 ns per window, yielding a total data collection time of 320 ns. A value of $K = 5$ kcal/mol was set to restrain ζ in all simulations. The weighted histogram analysis method (WHAM) [45] was used to unbiased simulations and to retrieve the PMF. Errors were estimated by the bootstrapping analysis implemented in the WHAM package [46].

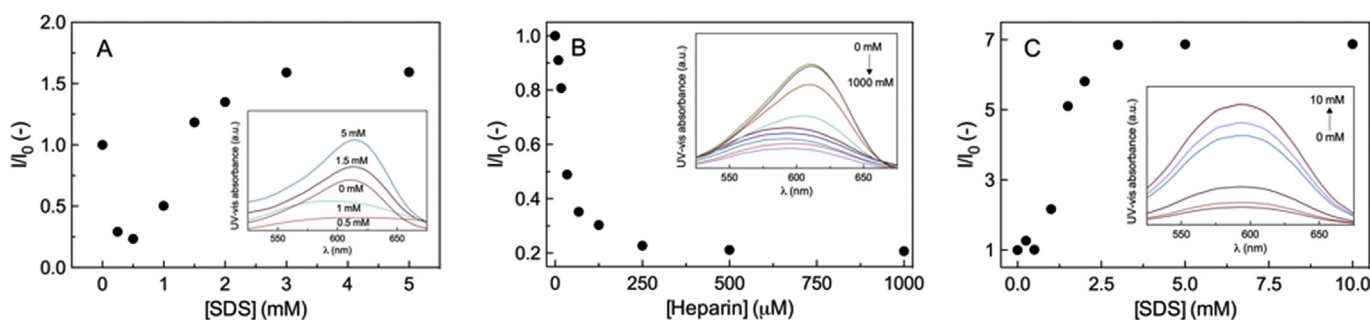


Fig. 2. Relative change in UV-visible absorbance intensity (I/I_0) of (A) MalB as a function of SDS concentration, (B) MalB as a function of heparin concentration, and (C) heparin/MalB complex as a function of SDS concentration in 10 mM Tris HCl and physiological ionic strength (150 mM NaCl). In all experiments, $[MalB] = 125 \mu M$. The corresponding absorbance spectra is shown in the relative Figure insets. For clarity, only a representative set of the corresponding absorbance spectra is shown in the inset of panel A (see Fig. S11 for the full curve set).

2.3.3. Mallard Blue/human serum albumin free energy of binding calculations

The free energy of binding between MalB and HSA was obtained by applying the Molecular Mechanics/Poisson Boltzmann Surface Area (MM/PBSA) approach [13–16]. This computational technique employs snapshots taken from MD trajectories to estimate the average interaction energies based on the solute molecular mechanics internal energy and solvation energy (constituting the enthalpic term), and entropy variation. The solvation term is calculated solving the Poisson-Boltzmann equation [47] while ΔG_{np} can be obtained via the semi-empirical expression [48]: $\Delta G_{np} = \gamma \times SASA + \beta$, in which SASA is the solvent accessible surface area of the molecule, γ is the surface tension parameter ($0.00542 \text{ kcal}/\text{\AA}^2/\text{mol}$), and $\beta = 0.92 \text{ kcal}/\text{mol}$. Finally, the entropic contribution is calculated via normal mode of harmonic frequencies [49] obtained from a subset of minimized snapshots taken from the corresponding MD trajectories. For the analysis of the energy of interaction between HSA and MalB, energy values were averaged over 200 frames taken during equally spaced time intervals along the last 15 ns of the MD production steps. Normal mode analysis was carried out on a subset of 15 minimized MD snapshots evenly extracted from the relevant trajectory time frame used for energy calculations.

3. Results and discussion

3.1. UV-visible spectroscopy assays

The first experiment was carried out to investigate the binding of MalB to SDS using UV-visible spectroscopy. The insert in Fig. 2A shows a representative set of the UV-visible spectra of MalB in the absence and in the presence of increasing concentration of SDS (the full curve set is shown in Fig. S11). As already reported in our previous investigation [7], MalB in 150 mM NaCl/10 mM Tris HCl buffer produces an absorption peak at 615 nm; upon addition of SDS, the maximum absorbance initially decreases and then increases with increasing surfactant concentration. This non-monotonic behavior can be better appreciated by plotting the relative change in absorption intensity (I/I_0 , where I and I_0 are the peak absorption values in the presence and absence of SDS, respectively), as illustrated in Fig. 2A.

We see from this Figure that, for small additions of SDS (i.e., $[SDS] < CMC_{SDS}$), I/I_0 attains values lower than 1. This initial quenching of the MalB UV-visible absorbance intensity can be attributed to the interaction of MalB molecules with SDS surfactant in its monomeric form, in agreement with previous literature reports for other cationic dyes, e.g., Nile Blue [50] and phenosafranine

[51]. As $[SDS]$ approaches CMC_{SDS} in the adopted buffer conditions ($CMC_{SDS} = 1.02 \text{ mM}$ in 150 mM NaCl/10 mM Tris HCl, see Fig. S12), I/I_0 rapidly increases and then levels-off for surfactant concentration values $> 3 \text{ mM}$ (Fig. 2A). The substantial increase in the absorption spectrum intensity of MalB at higher SDS concentrations is indicative of a tighter binding of the dye with SDS micelles driven by electrostatic forces between the highly negative micellar surface and the positive charges present on the molecular dye, which places MalB into a different environment [52–54].

Fig. 2B shows the profile of I/I_0 for the interaction between MalB and heparin. In this case, the initial electrostatic polyanion/MalB interactions result in a plummet of the MalB UV-visible absorption intensity, followed by a considerably less pronounced decrease of I/I_0 vs. $[Heparin]$ once all polysaccharide binding sites become saturated by dye binding (i.e., $125 \mu M < [Heparin] < 250 \mu M$). Interestingly, a similar behavior has been reported for Nile Blue binding to DNA [50,55], suggesting that common mechanisms may underlie the interactions of different cationic molecules with the two seemingly different, negatively charged biomacromolecules.

When SDS solutions are added to a pre-formed MalB/heparin complex, the UV-visible spectra reported in Fig. 2C are obtained. The initially flat curve of I/I_0 as a function of $[SDS]$ rapidly increases for $[SDS] \geq CMC_{SDS}$ and ultimately plateaus for $[SDS] > 2.5 \mu M$. In this last surfactant concentration range, the absorption intensity values correspond to those observed for MalB in the pure SDS micellar environment, strongly supporting the notion that the dye, no longer bound to heparin, has been complexed by the surfactant self-assembled spherical micelles.¹

3.2. Isothermal titration calorimetry (ITC) assays

To experimentally quantify - for the first time - the binding thermodynamics between MalB and heparin, to confirm the spectroscopic evidences of MalB/SDS micelle interactions, and to verify the ability of SDS micelles to extract MalB from heparin, we resorted to ITC measurements, as shown in Fig. 3.

The binding of MalB to heparin (Fig. 3A) is strongly exothermic ($\Delta H_b = -9.36 \pm 0.24 \text{ kcal}/\text{mol}$), while a small, negative entropy change opposes dye/polyanion interaction ($T\Delta S_b = -1.47 \text{ kcal}/\text{mol}$). Accordingly, MalB/heparin complex formation is thermodynamically favored, with a free energy of binding ΔG_b value of $-7.89 \text{ kcal}/\text{mol}$ (see Fig. 4A). The large, negative enthalpy variation observed in

¹ It should be noted that the I/I_0 value appears larger in Fig. 2C than 2A because the starting point of the experiment, and hence the value of I_0 , is different. In Fig. 2A the starting point I_0 value corresponds to uncomplexed MalB, whereas in Fig. 2B, the starting point I_0 corresponds to MalB bound to heparin.

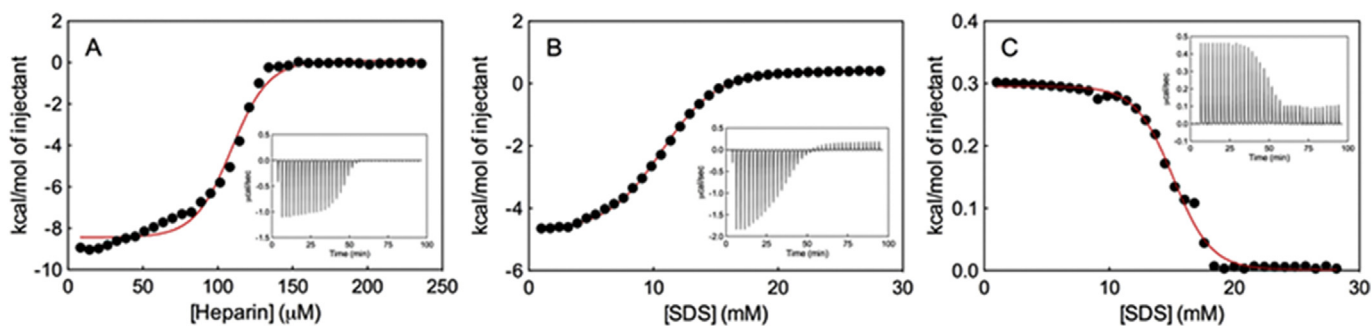


Fig. 3. Representative integrated ITC profiles for titration of (A) MalB with heparin, (B) MalB with SDS, and (C) MalB/heparin complex with SDS in 10 mM Tris HCl and physiological ionic strength (150 mM NaCl). $T = 25\text{ }^{\circ}\text{C}$. The solid red lines are data fitting with a sigmoidal function. The inserts in each panel show the corresponding ITC raw data. All experiments were run in triplicate. (For interpretation of the references to colour in this figure legend, the reader is referred to the web version of this article.)

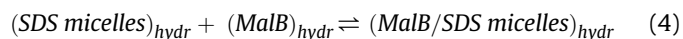
MalB/heparin complex formation is comparable to that observed for, e.g., small molecule/DNA or drug/protein binding [9–22,26–34], and can be ascribed to the formation of a network of stabilizing non-specific intermolecular interactions (i.e., electrostatic, hydrogen bonds, salt bridges) between the two molecular entities. The small and unfavorable entropic term is also quite characteristic of these processes, since macromolecule/ligand hydrophobic interactions and water/ion release into the bulk cannot compensate for the loss in degree of freedom of experienced by the dye/polyanion upon binding.

The interaction of SDS micelles with MalB (Fig. 3B) is also enthalpically driven ($\Delta H_b = -9.06 \pm 0.19$ kcal/mol) and, as for MalB/heparin binding, is characterized by a small entropic penalty ($T\Delta S_b = -1.64$ kcal/mol), resulting in an overall favorable binding free energy ΔG_b of -7.42 kcal/mol (Fig. 4B). The fact that the MalB/SDS has a substantial enthalpic nature supports the fact that hydrophobic interactions contribute only in minimal part to this specific dye/micelle binding, and electrostatic forces play the leading role. This, in turn, suggests that, once bound, MalB prefers to reside in the micellar outer Stern layer rather than locating itself into the palisade layer or deep inside the micellar core (see Section 3.3).

Finally, ITC measurements reveal that, when SDS micelles are added to a MalB/heparin complex solution, the thermodynamic nature of the underlying process is opposite with respect to that described above (Fig. 3C). Indeed, while an almost negligible, endothermic contribution is measured ($\Delta H_b = +0.23 \pm 0.04$ kcal/mol), the driving force for MalB extraction from heparin by SDS micelles results from the strong, positive entropic variation ($T\Delta S_b = +6.25$ kcal/mol), which ultimately determines the overall negative value of the free energy ($\Delta G_b = -6.02$ kcal/mol) (see

Fig. 4C). The increase in system entropy can be attributed to several, concomitant factors, including i) an increase in degrees of freedom of heparin after MalB complexation, ii) the disruption of hydrogen bonds and electrostatic interactions between water molecules/counterions and the micellar surface upon MalB binding, and iii) their subsequent release into the bulk solvent.

In order to model the process of MalB extraction from heparin by the anionic surfactant micelles the following two-step model can be assumed:



in which all different species are considered in their hydrated form in the relevant buffer. The approach is obviously a rough simplification of reality, as i) it assumes that Eqs. (3) and (4) represent independent events and ii) additional steps associated with these two major events either do not contribute significantly to the overall process or their effects are accounted for by the equilibrium thermodynamic parameters. Under this hypothesis, and with the further assumption that each binding process is reversible, the unbinding of MalB from heparin (i.e., Eq. (3)) should then be characterized by a positive enthalpic contribution of $+9.36$ kcal/mol (i.e., $-\Delta H_b$ in Figs. 3A and 4A). Since Eq. (4) represents the direct titration of MalB with SDS micelles, the enthalpic term corresponds to $\Delta H_b = -9.06$ kcal/mol (Figs. 3B and 4B). Thus, for the extraction of MalB from its heparin complex by SDS micelles an endothermic contribution of $+0.30$ kcal/mol (viz, $+9.36 - 9.06$ kcal/mol) is estimated, which matches the experimental $+0.23$ kcal/mol directly measured by ITC, as discussed above (Fig. 4C). The nice agreement

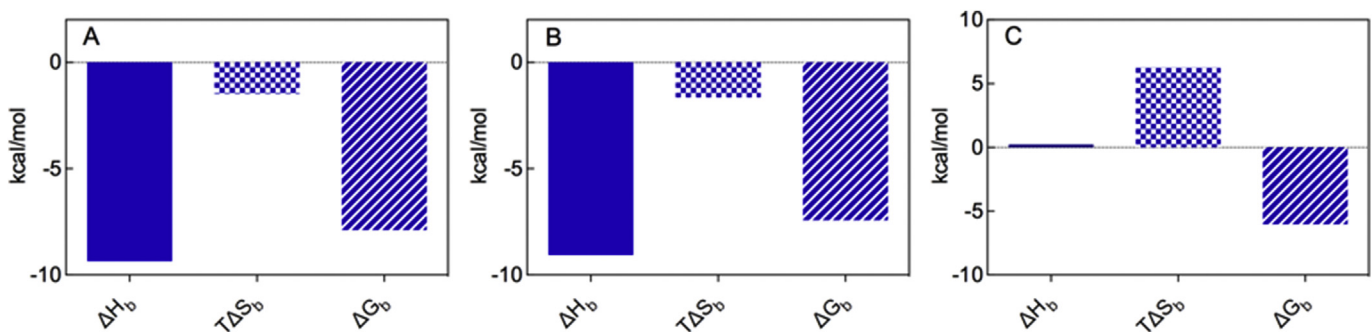


Fig. 4. ITC-derived thermodynamic parameters (ΔH_b , full color; $T\Delta S_b$, square pattern; ΔG_b , diagonal line pattern) for (A) MalB binding with heparin, (B) MalB binding with SDS, and (C) extraction of MalB from the MalB/heparin complex with SDS. (For interpretation of the references to colour in this figure legend, the reader is referred to the web version of this article.)

between the results obtained from the model of SDS-driven MalB decomplexation from heparin and the relevant experimental data, means we can conclude that the underlying assumption that two processes described by Eqs. (3) and (4) indeed take place in successive steps.

3.3. Steered molecular dynamics (SMD) and umbrella sampling (US) of MalB/SDS micelle binding

To obtain a molecular view of the ITC data discussed in Section 3.2, we performed computer-based simulations by using SMD and US simulations. In our case, SMD is used first to pull out MalB from heparin (see Supplementary Material Movie1) and then to drive its binding onto a SDS micelle (Supplementary Material Movie2), by applying a guiding potential along a reaction coordinate ζ , and is subsequently employed to generate the initial coordinate for the umbrella sampling computations. Upon US simulations to enhance extensive sampling along the reaction coordinate, the potential of mean force (PMF) of the binding/unbinding process can be constructed.

Supplementary video related to this article can be found at <https://doi.org/10.1016/j.fluid.2017.11.005>.

Fig. 5A illustrates the PMF profile as a function of the reaction coordinate ζ for the unbinding process of MalB from heparin. As seen in this Figure, the PMF continually increases as the pulled MalB transits from the bound to the free state, although some bumpy features are visible along the pathway. These might be related to the fact that the 5 positive charges on MalB are progressively detached from the polyanion and become solvated by water molecules and neutralizing counterions. The total free energy difference between the heparin bound and unbound state of MalB is 8.10 kcal/mol, in good agreement with the corresponding free energy of binding measured by ITC (-7.89 kcal/mol, Fig. 4A).

Fig. 5B displays the PMF (ζ) behavior for the binding of MalB to the SDS micelle. This Figure shows that the corresponding free energy minimum is located on the micellar surface, at a distance of ~ 1.8 nm from the center of its core. As ζ is further decreased, the PMF increases steadily. This strongly supports the hypothesis formulated in Section 3.2, according to which, once bound, the highly positively-charged MalB molecule does not penetrate the palisade layer but remains anchored at the oppositely-charged micellar periphery by virtue of strong, stabilizing electrostatic interactions. The ultimate evidence of surface binding of MalB onto

the micellar surface is given by the Dynamic Light Scattering (DLS) experiments (see Supporting Information). According to DLS, SDS assembles in spherical micelles with a hydrodynamic diameter of ~ 4 nm (see insert in figure S13), characterized by a zeta potential of -63.2 ± 3.1 mV. Upon MalB interaction, the average hydrodynamic diameter is equal to ~ 4.8 nm (see figure S13) with a zeta-potential of -52.4 ± 3.7 mV, supporting the fact that SDS micelles/MalB binding takes place at the SDS micellar surface. Finally, the computed free energy changes associated with the MalB/SDS binding process, i.e., -7.96 kcal/mol, nicely matches the corresponding ITC-derived value of -7.42 kcal/mol (Fig. 4B).

3.4. Binding thermodynamics of MalB to HSA

One of the most important results previously reported for MalB as a heparin sensor is that, despite the fact that electrostatics should govern the interaction between the dye and the polyanion, the former is able to recognize heparin even in the presence of high ionic strength, and shows a quantitative linear dose-response behavior in serum [7]. Human serum albumin is the most abundant ($>50\%$) protein in blood plasma and serves as a depot protein and transport protein for numerous endogenous and exogenous compounds. HSA is also the main factor in contributing to the colloid osmotic pressure of the blood and has been suggested as a possible source of amino acids for various tissues. Indubitably, albumin is the most multifunctional transport protein and plays an important role in the transport and deposition of a variety of endogenous and exogenous substances in blood [56]. For these reasons, HSA has been considered as a simplified model in studying interaction and binding of drugs and small molecules with plasma proteins.

Under this perspective, we decided to quantify for the first time the interaction of MalB with HSA. To this purpose, we resorted again to a combination of experimental and computational methods. Fig. 6A reports the ITC results of the MalB/HSA binding, while panel B of the same Figure shows the comparison between the main dye/protein thermodynamic parameters as derived from ITC and MM/PBSA-based molecular dynamics simulations.

Several considerations can be drawn from the analysis of the data reported in Fig. 6. First, MalB is endowed with a substantially lower experimental affinity for HSA ($\Delta G_b = -5.99$ kcal/mol) than for heparin ($\Delta G_b = -7.89$ kcal/mol) or SDS ($\Delta G_b = -7.42$ kcal/mol) (see Fig. 4). The enthalpic change upon MalB/HSA complex

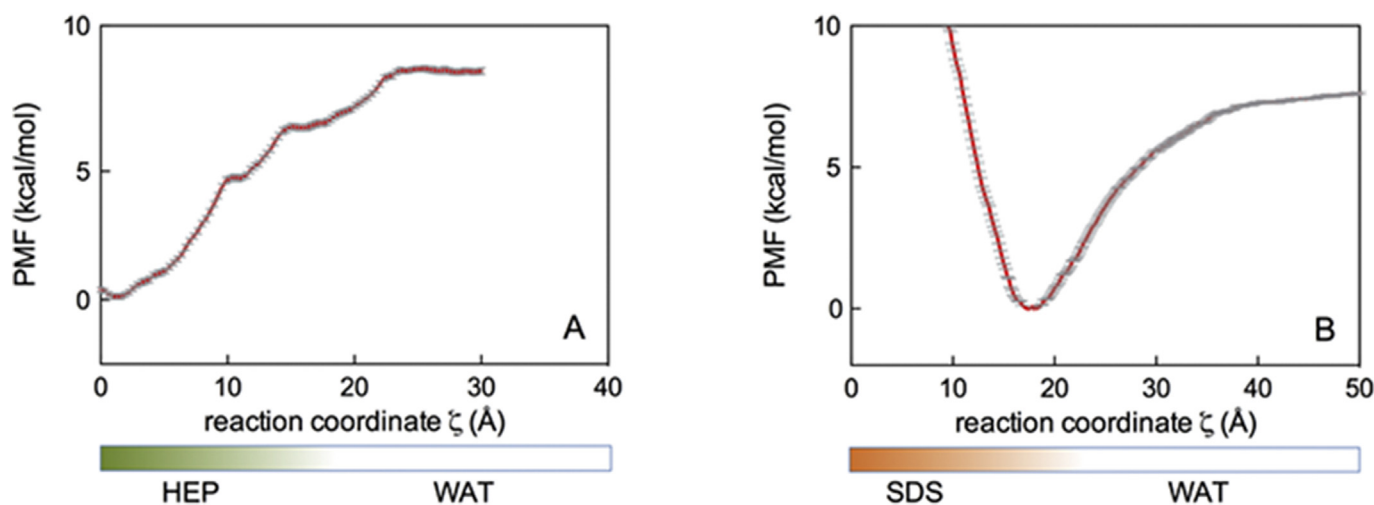


Fig. 5. PMF profile along the reaction coordinate ζ for the process of (A) unbinding of MalB from heparin and (B) binding of MalB to a SDS micelle.

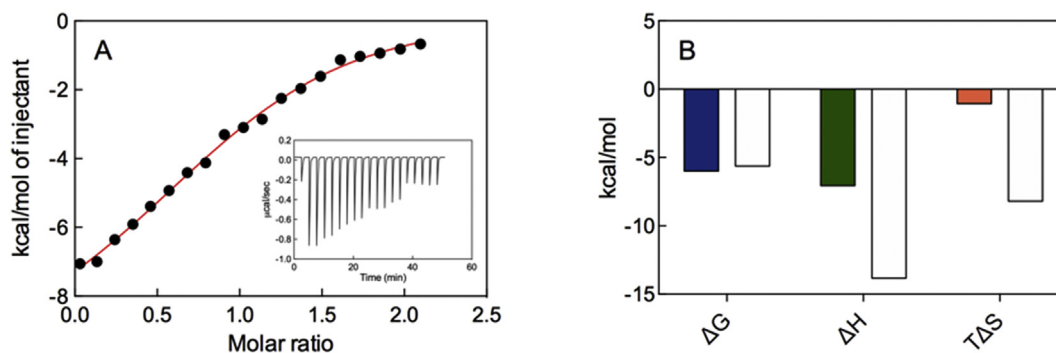


Fig. 6. (A) Integrated ITC profiles for MalB binding with HSA with in 10 mM Tris HCl and physiological ionic strength (150 mM NaCl). $T = 25^\circ\text{C}$. The solid red line is data fitting with a one-set-of-sites model. The insert in panel A shows the corresponding ITC raw data. Experiments were run in triplicate. (B) Comparison of ITC-derived (colored bars) and *in silico* predicted (white bars) thermodynamic parameters for MalB binding with HSA. (For interpretation of the references to colour in this figure legend, the reader is referred to the web version of this article.)

formation is favorable (-7.05 ± 0.12 kcal/mol) whereas the entropy change opposes binding (-1.06 kcal/mol) (Fig. 6B). The conformational entropy change is commonly unfavorable in protein-ligand binding event, as the binding process involves the loss of configurational degrees of freedom for both the drug molecule and the protein. However, the entropic penalty paid by the small dye upon protein binding is largely compensated by the corresponding enthalpic gain (Fig. 6B), thereby confirming the enthalpic-driven nature of the binding mechanism of MalB to human serum albumin. From the computational standpoint, MalB docking onto HSA (Fig. 7, left panel) followed by free energy of binding scoring in the framework of the MM/PBSA methodology results in a calculated $\Delta G_{b,comp}$ value in excellent agreement (-5.63 kcal/mol) with the corresponding ITC-derived experimental data (-5.99 kcal/mol), as illustrated in Fig. 6B. The enthalpic nature of MalB/HSA is confirmed computationally (-13.82 kcal/mol), as is the unfavorable contribution from entropy variation upon binding (-8.19 kcal/mol). It is important to observe here that both ΔH_b and $T\Delta S_b$ are normally overestimated in MM/PBSA calculations [37], as in the present case; yet, a parallel shift is generally observed between experimental and computed ΔH and $-T\Delta S$ so that, ultimately, their difference is indeed close to the relevant experimental value. The analysis of the MD trajectory for the MalB/HSA complex shows that the dye is engaged in two permanent salt bridges, involving the negatively

charged side chains of residues Glu379 and Glu593 on the protein side and one guanidinic and one tertiary amines of the dye, respectively (Fig. 7, right panel). The intermolecular complex is further stabilized by two hydrogen bonds that, in a symmetrical fashion, link the second guanidinic and tertiary amines to the side chains of Asn383 and Gln394. Finally, residues Leu384, Leu391, and Ala403 contribute favorable hydrophobic interactions to dye/protein binding (Fig. 7, right panel).

In aggregate, these data quantitatively support our previous evidence [7], according to which MalB can overcome one of the major challenges for heparin sensors (i.e., working in complex biological fluids), ultimately making it superior to some other approaches.

4. Conclusions

Heparin, one of the most negatively charged biopolymers, plays a critical role in the regulation of blood coagulation, cell growth, and immune response. Moreover, overdose of heparin frequently induced severe side effects such as hemorrhage, thrombocytopenia, and osteoporosis. Thus, the selective and sensitive detection of heparin, is of great importance in general medicine and clinical settings. In recent years, our group has developed Mallard Blue (MalB) [7], a new heparin-binding dye that binds heparin in highly competitive media, including water with high levels of competitive electrolyte, buffered aqueous solution and human serum, and simply reports on heparin levels by a significant change in its UV-visible spectroscopic profile. However, several aspects remain to be explored about the interaction of MalB with its target polyanion, and their unveiling will undoubtedly influence how MalB will be eventually used in biomedical and pharmacological contexts.

In this work, we investigated some of these unexplored issues, namely the thermodynamics of binding between MalB and heparin, and the eventual negative interference by the most abundant plasma proteins, namely human serum albumin (HSA), in the MalB/heparin complex formation. Also, in analogy with what is observed for, e.g., DNA and small intercalating molecules, we deemed it interesting to study the competition for MalB binding by other polyanions, such negatively-charged sodium dodecyl sulfate (SDS) micelles. To this purpose, we adopted an integrated approach based on a combination of experimental and computational technique.

The results obtained from the application of UV-visible spectroscopy methods allowed us to establish that, in a common buffer system (150 mM NaCl/10 mM Tris HCl), MalB efficiently binds to both heparin and SDS; yet, SDS is able to extract MalB from its complex with heparin when the surfactant is in its self-assembled

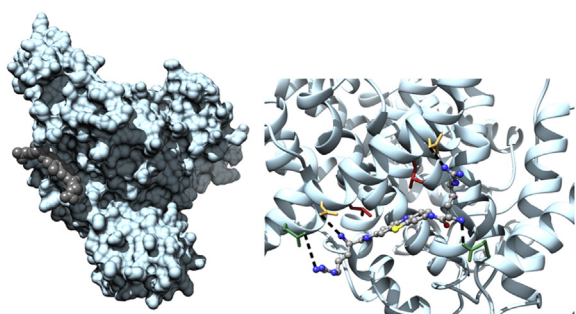


Fig. 7. (Left) Overall space filling representation of the HSA molecular surface (light blue) and MalB (gray spheres) docked into the protein binding site. (Right) Details of MalB in the HSA binding pocket. The protein secondary structure is portrayed in a light blue-ribbon style, while MalB is shown as atom-colored sticks-and-balls (C, gray; N, blue; O, red; S, yellow). The side chains of the HSA residues mainly involved in MalB binding are shown as colored sticks, colored according to the underlying interactions (salt bridges, sea green; hydrogen bonds, sandy brown; hydrophobic interactions, firebrick). Hydrogen atoms, counterions, and water molecules are omitted for clarity. (For interpretation of the references to colour in this figure legend, the reader is referred to the web version of this article.)

form (Fig. 2). Accordingly, in this paper we demonstrate, for the first time, that small, positively charged molecules bound to heparin, the most negatively charged polyanion existing in nature, can be “sequestered” by anionic nanomicelles in a way that utterly resembles that seen for DNA. Moreover, given the fundamental electrostatic nature of MalB/SDS interactions, once bound the dye remains anchored to the micellar surface and does not penetrate into the micelle palisade layer, as further confirmed by computational results. Indeed, the minimum of the potential of mean force for MalB/SDS binding is located at a distance matching the radius of the surfactant micelle (1.80 nm), and further pulling of MalB towards the center of the micelle results in a steep increase of the free energy (Fig. 5). UV-vis results are supported by isothermal titration calorimetry (ITC) measurements, according to which heparin and SDS have similar affinity for the dye, and in both cases favorable enthalpy variations drive the underlying processes (Fig. 4). On the other hand, the “extraction” of MalB from heparin by SDS micelles is thermodynamically feasible since the major driving force of the process is purely entropic in nature, with the enthalpies of binding to each of these polyanions effectively canceling one another out. Finally, the investigation of the interaction between MalB and human serum albumin (HSA) reveals that the dye is endowed with substantially less affinity for the most abundant plasma proteins compared with its affinity for heparin (Fig. 6), confirming the ability of this heparin dye to work in complex physiological environments.

Acknowledgments

The work has been financially supported by the Italian Association for Cancer Research (AIRC, IG 2015 ID.17413 to SP).

References

- [1] D.A. Lane, U. Lindhal (Eds.), *Heparin: Chemical and Biological Properties, Clinical Applications*, CRC Press, Boca Raton, FL, 1989.
- [2] M.D. Klein, R.A. Drongowski, R.J. Linhardt, R.S. Langer, A colorimetric assay for chemical heparin in plasma, *Anal. Biochem.* 124 (1982) 59–64.
- [3] Q.C. Jiao, Q. Liu, Mechanism of interference and Azure A response in the heparin assay, *Anal. Lett.* 31 (1998) 1311–1323.
- [4] S.B. Frazier, K.A. Roodhouse, D.E. Hourcade, L. Zhang, The quantification of glycosaminoglycans: a comparison of HPLC, carbazole, and Alcian Blue methods, *Open Glycosci.* 1 (2008) 31–39.
- [5] Q.C. Jiao, Q. Liu, C. Sun, H. He, Investigation on the binding site in heparin by spectrophotometry, *Talanta* 48 (1999) 1095–1101.
- [6] S. Wang, Y.T. Chang, Discovery of heparin chemosensors through diversity oriented fluorescence library approach, *Chem. Commun.* 14 (2008) 1173–1175.
- [7] S.M. Bromfield, A. Barnard, P. Posocco, M. Fermeglia, S. Pricl, D.K. Smith, Mallard Blue: a high-affinity selective heparin sensor that operates in highly competitive media, *J. Am. Chem. Soc.* 135 (2013) 2911–2914.
- [8] Z. Shriver, R. Sasisekharan, Blue-chip binding, *Nat. Chem.* 5 (2013) 644–646.
- [9] E. Laurini, D. Marson, P. Posocco, M. Fermeglia, S. Pricl, Structure and binding thermodynamics of viologen-phosphorous dendrimers to human serum albumin: a combined computational/experimental investigation, *Fluid Phase Equilib.* 422 (2016) 18–31.
- [10] D. Marson, E. Laurini, P. Posocco, M. Fermeglia, S. Pricl, Cationic carboxylate dendrimers and oligonucleotide binding: an energetic affair, *Nanoscale* 7 (2015) 3876–3887.
- [11] S. Pricl, B. Cortelazzi, V. Dal Col, D. Marson, E. Laurini, M. Fermeglia, L. Licitra, S. Pilotti, P. Bossi, F. Perrone, Smoothed (SMO) receptor mutations dictate resistance to vismodegib in basal cell carcinoma, *Mol. Oncol.* 9 (2015) 389–397.
- [12] F. Bozzi, E. Conca, E. Laurini, P. Posocco, A. Lo Sardo, G. Jocolle, R. Sanfilippo, A. Gronchi, F. Perrone, E. Tamborini, G. Pelosi, M.A. Pierotti, R. Maestro, S. Pricl, S. Pilotti, In vitro and in silico studies of MDM2/MDMX isoforms predict Nutlin-3A sensitivity in well/differentiated liposarcomas, *Lab. Invest.* 93 (2013) 1232–1240.
- [13] D. Genini, L. Brambilla, E. Laurini, J. Merulla, G. Civenni, S. Pandit, R. D’Antuono, L. Perez, D.E. Levy, S. Pricl, G.M. Carbone, C.V. Catapano, Mitochondrial dysfunction induced by a SH2 domain-targeting STAT3 inhibitor leads to metabolic synthetic lethality in cancer cells, *Proc. Natl. Acad. Sci. U. S. A.* 2017 114 (2017) E4924–E4933.
- [14] Z. Beiranvand, F. Bani, A. Kakanejadifard, E. Laurini, M. Fermeglia, S. Pricl, M. Adeli, Anticancer drug delivery systems based on specific interactions between albumin and polyglycerol, *RSC Adv.* 6 (2016) 11266–11277.
- [15] D.L. Gibbons, S. Pricl, P. Posocco, E. Laurini, M. Fermeglia, H. Sun, M. Talpaz, N.J. Donato, A. Quintás-Cardama, Molecular dynamics reveal BCR-ABL1 polymutants as a unique mechanism of resistance to PAN-BCR-ABL1 kinase inhibitor therapy, *Proc. Natl. Acad. Sci. U. S. A.* 111 (2014) 3550–3555.
- [16] M.A. Pierotti, E. Tamborini, T. Negri, S. Pricl, S. Pilotti, Targeted therapy in GIST: in silico modeling for prediction of resistance, *Nat. Rev. Clin. Oncol.* 8 (2011) 161–170.
- [17] A.C. Rodrigo, S.M. Bromfield, E. Laurini, P. Posocco, S. Pricl, D.K. Smith, Morphological control of self-assembled multivalent (SAMul) heparin binding in highly competitive media, *Chem. Commun.* 53 (2017) 6335–6338.
- [18] V.M.P. Vieira, V. Liljeström, P. Posocco, E. Laurini, S. Pricl, M.A. Kostianen, D.K. Smith, Emergence of highly-ordered hierarchical nanoscale aggregates on electrostatic binding of self-assembled multivalent (SAMul) cationic micelles with polyanionic heparin, *J. Mater. Chem. B* 5 (2017) 341–347.
- [19] C.W. Chan, E. Laurini, P. Posocco, S. Pricl, D.K. Smith, Chiral recognition at self-assembled multivalent (SAMul) nanoscale interfaces – enantioselectivity in polyanion binding, *Chem. Commun.* 52 (2016) 10540–10543.
- [20] L.E. Fechner, B. Albanyan, V.M.P. Vieira, E. Laurini, P. Posocco, S. Pricl, D.K. Smith, Electrostatic binding of polyanions using self-assembled multivalent (SAMul) ligand displays-structure-activity effects on DNA/heparin binding, *Chem. Sci.* 7 (2016) 4653–4659.
- [21] S.M. Bromfield, P. Posocco, C.W. Chan, M. Calderon, S.E. Guimond, J.E. Turnbull, S. Pricl, D.K. Smith, Nanoscale self-assembled multivalent (SAMul) heparin binders in highly competitive, biologically relevant, aqueous media, *Chem. Sci.* 5 (2014) 1484–1492.
- [22] S.M. Bromfield, P. Posocco, M. Fermeglia, S. Pricl, J. Rodríguez-López, D.K. Smith, A simple new competition assay for heparin binding in serum applied to multivalent PAMAM dendrimers, *Chem. Commun.* 49 (2013) 4830–4832.
- [23] D.A. Case, R.M. Betz, W. Botello-Smith, D.S. Cerutti, T.E. Cheatham III, T.A. Darden, R.E. Duke, T.J. Giese, H. Gohlke, A.W. Goetz, N. Homeyer, S. Izadi, P. Janowski, et al., *AMBER 2016*, University of California, San Francisco (CA, USA), 2016.
- [24] J. Wang, R.M. Wolf, J.W. Caldwell, P.A. Kollman, D.A. Case, Development and testing of a general amber force field, *J. Comput. Chem.* 25 (2004) 1157–1174.
- [25] www.micelle.icm.uu.se.
- [26] B. Albanyan, E. Laurini, P. Posocco, S. Pricl, D.K. Smith, Self-assembled multivalent (SAMul) polyanion binding-impact of hydrophobic modifications in the micellar core on DNA and heparin binding at the peripheral cationic ligands, *Chem. Eur. J.* 23 (2017) 6391–6397.
- [27] C. Chen, P. Posocco, X. Liu, Q. Cheng, E. Laurini, J. Zhou, C. Liu, Y. Wang, J. Tang, V. Dal Col, T. Yu, S. Giorgio, M. Fermeglia, F. Qu, Z. Liang, J.J. Rossi, M. Liu, P. Rocchi, S. Pricl, L. Peng, Mastering dendrimer self-assembly for efficient siRNA delivery: from conceptual design to in vivo efficient gene silencing, *Small* 12 (2016) 3667–3676.
- [28] T. Wei, C. Chen, J. Liu, C. Liu, P. Posocco, X. Liu, Q. Cheng, S. Huo, Z. Liang, M. Fermeglia, S. Pricl, X.J. Liang, P. Rocchi, L. Peng, Anticancer drug nanomicelles formed by self-assembling amphiphilic dendrimer to combat cancer drug resistance, *Proc. Natl. Acad. Sci. U. S. A.* 112 (2015) 2978–2983.
- [29] X. Liu, J. Zhou, T. Yu, C. Chen, Q. Cheng, K. Sengupta, Y. Huang, H. Li, C. Liu, Y. Wang, P. Posocco, M. Wang, Q. Cui, S. Giorgio, M. Fermeglia, F. Qu, S. Pricl, Y. Shi, Z. Liang, P. Rocchi, J.J. Rossi, L. Peng, Adaptive amphiphilic dendrimer-based nanoassemblies as robust and versatile siRNA delivery systems, *Angew. Chem. Int. Ed. Engl.* 53 (2014) 11822–11827.
- [30] A. Barnard, P. Posocco, S. Pricl, M. Calderon, R. Haag, M.E. Hwang, V.W. Shum, D.W. Pack, D.K. Smith, Degradable self-assembling dendrons for gene delivery: experimental and theoretical insights into the barriers to cellular uptake, *J. Am. Chem. Soc.* 133 (2011) 20288–20300.
- [31] V. Perfetti, E. Laurini, S. Aulić, M. Fermeglia, R. Riboni, M. Lucioni, E. Dallera, S. Delfanti, L. Pugliese, F.S. Latteri, A. Pietrabissa, S. Pricl, Molecular and functional characterization of a new 3’ end KIT juxtamembrane deletion in a duodenal GIST treated with neoadjuvant Imatinib, *Oncotarget* 8 (2017) 56158–56167.
- [32] A.K. Kokornaczyk, D. Schepmann, J. Yamaguchi, K. Itami, E. Laurini, M. Fermeglia, S. Pricl, B. Wünsch, Thiazole-based $\sigma 1$ receptor ligands: diversity by late-stage C-H arylation of thiazoles, structure-affinity and selectivity relationships, and molecular interactions, *ChemMedChem* 12 (2017) 1070–1080.
- [33] D. Zampieri, L. Vio, M. Fermeglia, S. Pricl, B. Wünsch, D. Schepmann, M. Romano, M.G. Mamolo, E. Laurini, Computer-assisted design, synthesis, binding and cytotoxicity assessments of new 1-(4-(aryl(methyl)amino)butyl)-heterocyclic sigma 1 ligands, *Eur. J. Med. Chem.* 121 (2016) 712–726.
- [34] A. Carta, I. Briguglio, S. Piras, P. Corona, R. Ibba, E. Laurini, M. Fermeglia, S. Pricl, N. Desideri, E.M. Atzori, P. La Colla, G. Collu, I. Delogu, R. Loddò, A combined in silico/in vitro approach unveils common molecular requirements for efficient BVDV RdRp binding of linear aromatic N-polycyclic systems, *Eur. J. Med. Chem.* 117 (2016) 321–334.
- [35] G.M. Morris, R. Huey, W. Lindstrom, M.F. Sanner, R.K. Belew, D.S. Goodsell,

- A.J. Olson, AutoDock4 and AutoDockTools4: automated docking with selective receptor flexibility, *J. Comput. Chem.* 30 (2009) 2785–2791.
- [36] C. Meyer, D. Schepmann, S. Yanagisawa, J. Yamaguchi, V. Dal Col, E. Laurini, K. Itami, S. Pricl, B. Wünsch, Pd-catalyzed direct C-H bond functionalization of spirocyclic sigma-1 ligands: generation of a pharmacophore model and analysis of reverse binding mode by docking into a 3D homology model of the sigma-1 receptor, *J. Med. Chem.* 55 (2012) 8047–8065.
- [37] D. Rossi, A. Pedrali, R. Gaggeri, A. Marra, L. Pignataro, E. Laurini, V. Dal Col, E. Fermeglia, S. Pricl, D. Schepmann, B. Wünsch, M. Peviani, D. Curti, S. Collina, Chemical, pharmacological, and in vitro metabolic stability studies on enantiomerically pure RC-33 compounds: promising neuroprotective agents acting as σ_1 receptor agonists, *ChemMedChem* 8 (2013) 1514–1527.
- [38] E. Laurini, D. Harel, D. Marson, D. Schepmann, T. Schmidt, S. Pricl, B. Wünsch, Identification, pharmacological evaluation and binding mode analysis of novel chromene and chromane based σ_1 receptor ligands, *Eur. J. Med. Chem.* 83 (2014) 526–533.
- [39] W.L. Jorgensen, J. Chandrasekhar, J.D. Madura, R.W. Impey, M.L. Klein, Comparison of simple potential functions for simulating liquid water, *J. Chem. Phys.* 79 (1983) 926–935.
- [40] J.P. Ryckaert, G. Ciccotti, H.J.C. Berendsen, Numerical integration of the cartesian equations of motion of a system with constraints: molecular dynamics of n-alkanes, *J. Comput. Phys.* 23 (1977) 327–341.
- [41] X. Wu, B.R. Brooks, Self-guided Langevin dynamics simulation method, *Chem. Phys. Lett.* 381 (2003) 512–518.
- [42] H.J.C. Berendsen, J.P.M. Postma, W.F. van Gunsteren, A. DiNola, J.R. Haak, Molecular dynamics with coupling to an external bath, *J. Chem. Phys.* 81 (1984) 3684–3690.
- [43] T. Darden, D. York, L. Pedersen, Particle mesh Ewald: an N log(N) method for Ewald sums in large systems, *J. Chem. Phys.* 98 (1993) 10089–10092.
- [44] J. Kästner, Umbrella sampling, *WIREs* 1 (2011) 932–942.
- [45] S. Kumar, D. Bouzida, R.H. Swendsen, P.A. Kollman, J.M. Rosenberg, The weighted histogram analysis method for free-energy calculations on biomolecules. I. The method, *J. Comput. Chem.* 13 (1992) 1011–1021.
- [46] <http://membrane.urmc.rochester.edu/content/wham>.
- [47] M.K. Gilson, K.A. Sharp, B.H. Honig, Calculating the electrostatic potential of molecules in solution: a method and error assessment, *J. Comput. Chem.* 9 (1988) 327–335.
- [48] D. Sitkoff, K.A. Sharp, B.H. Honig, Accurate calculation of hydration free energies using macroscopic solvent models, *J. Phys. Chem.* 98 (1994) 1978–1988.
- [49] I. Andricioaei, M. Karplus, On the calculation of entropy from covariance matrices of the atomic fluctuations, *J. Chem. Phys.* 115 (2001) 6289–6292.
- [50] R.K. Mitra, S.S. Sinha, S.K. Pal, Interactions of Nile Blue with micelles, reverse micelles and a genomic DNA, *J. Fluoresc.* 18 (2008) 423–432.
- [51] A. Patra, S. Hazra, G.S. Kumar, R.K. Mitra, Entropy contribution toward micelle-driven deintercalation of drug–DNA complex, *J. Phys. Chem. B* 118 (2014) 901–908.
- [52] P. Das, A. Chakrabarty, A. Mallick, N. Chattopadhyay, Photophysics of a cationic biological photosensitizer in anionic micellar environments: combined effect of polarity and rigidity, *J. Phys. Chem. B* 111 (2007) 11169–11176.
- [53] M. Afzal, S. Ghosh, S. Das, N. Chattopadhyay, Endogenous activation-induced delivery of a bioactive photosensitizer from a micellar carrier to natural DNA, *J. Phys. Chem. B* 120 (2016) 11492–11501.
- [54] S. Chatterjee, G.S. Kumar, Visualization of stepwise drug-micelle aggregate formation and correlation with spectroscopic and calorimetric results, *J. Phys. Chem. B* 120 (2016) 11751–11760.
- [55] R.K. Mitra, S.S. Sinha, S. Maiti, S.K. Pal, Sequence dependent ultrafast electron transfer of Nile Blue in oligonucleotides, *J. Fluoresc.* 19 (2009) 353–361.
- [56] G. Fanali, A. di Masi, V. Trezza, M. Marino, M. Fasano, P. Ascenzi, Human serum albumin: from bench to bedside, *Mol. Asp. Med.* 33 (2012) 209–290.